JACS
JOURNAL OF THE AMERICAN CHEMICAL SOCIETY

Subscriber access provided by CARLETON UNIVERSITY

Article

Planar plus twisted molecular structure leads to high brightness of semiconducting polymer nanoparticles for NIR-IIa fluorescence imaging

Shunjie Liu, Hanlin Ou, Yuanyuan Li, Haoke Zhang, Junkai Liu, Xuefeng Lu, Ryan T. K. Kwok, Jacky W. Y. Lam, Dan Ding, and Ben Zhong Tang

J. Am. Chem. Soc., **Just Accepted Manuscript** • DOI: 10.1021/jacs.0c07193 • Publication Date (Web): 05 Aug 2020

Downloaded from pubs.acs.org on August 6, 2020

Just Accepted

"Just Accepted" manuscripts have been peer-reviewed and accepted for publication. They are posted online prior to technical editing, formatting for publication and author proofing. The American Chemical Society provides "Just Accepted" as a service to the research community to expedite the dissemination of scientific material as soon as possible after acceptance. "Just Accepted" manuscripts appear in full in PDF format accompanied by an HTML abstract. "Just Accepted" manuscripts have been fully peer reviewed, but should not be considered the official version of record. They are citable by the Digital Object Identifier (DOI®). "Just Accepted" is an optional service offered to authors. Therefore, the "Just Accepted" Web site may not include all articles that will be published in the journal. After a manuscript is technically edited and formatted, it will be removed from the "Just Accepted" Web site and published as an ASAP article. Note that technical editing may introduce minor changes to the manuscript text and/or graphics which could affect content, and all legal disclaimers and ethical guidelines that apply to the journal pertain. ACS cannot be held responsible for errors or consequences arising from the use of information contained in these "Just Accepted" manuscripts.

is published by the American Chemical Society. 1155 Sixteenth Street N.W., Washington, DC 20036
Published by American Chemical Society. Copyright © American Chemical Society. However, no copyright claim is made to original U.S. Government works, or works produced by employees of any Commonwealth realm Crown government in the course of their duties.

Planar plus twisted molecular structure leads to high brightness of semiconducting polymer nanoparticles for NIR-IIa fluorescence imaging

Shunjie Liu,[†,#] Hanlin Ou,[‡,#] Yuanyuan Li,[†] Haoke Zhang,[†] Junkai Liu,[†] Xuefeng Lu,[†] Ryan T.K. Kwok,[†] Jacky W.Y. Lam,[†] Dan Ding, *,[‡] Ben Zhong Tang*,[†,⊥,∥]

[†]Department of Chemistry, Hong Kong Branch of Chinese National Engineering Research Center for Tissue Restoration and Reconstruction, Division of Life Science and State Key Laboratory of Molecular Neuroscience, and Division of Biomedical Engineering, The Hong Kong University of Science and Technology, Clear Water Bay, Kowloon, Hong Kong, China

[‡]State Key Laboratory of Medicinal Chemical Biology, Key Laboratory of Bioactive Materials, Ministry of Education, and College of Life Sciences, Nankai University, Tianjin 300071, China

[⊥]HKUST-Shenzhen Research Institute, No. 9 Yuexing 1st RD, South Area, Hi-tech Park, Nanshan, Shenzhen 518057, China

[∥]Center for Aggregation-Induced Emission, SCUT-HKUST Joint Research Institute, State Key Laboratory of Luminescent Materials and Devices, South China University of Technology, Guangzhou 510640, China

Abstract

Semiconducting polymer nanoparticles (SPNs) emitting in the second near-infrared window (NIR-II, 1000-1700 nm) are promising materials for deep-tissue optical imaging in mammals, but the brightness is far from satisfaction. Herein, we developed a molecular design strategy to boost the brightness of NIR-II SPNs: structure planarization and twisting. By integration of the strong absorption coefficient inherited from planar π-conjugated units and high solid-state quantum yield (Φ_{PL}) from twisted motifs into one polymer, a rise in brightness was obtained. The resulting pNIR-4 with both twisted and planar structure displayed improved Φ_{PL} and absorption than the planar polymer pNIR-1 and twisted polymer pNIR-2. Given the emission tail extending into the NIR-IIa region (1300-1400 nm) of pNIR-4 nanoparticles, NIR-IIa fluorescence imaging of blood vessels with enhanced clarity was observed. Moreover, a pH-responsive poly(*β*-amino ester) made pNIR-4 specifically accumulate at tumor sites, allowing NIR-IIa fluorescence image-guided cancer precision resection. This study provides a molecular design strategy for developing highly bright fluorophores.

Introduction

In vivo fluorescence imaging in the NIR-II region (1000-1700 nm) benefits from reduced photon scattering and minimized tissue autofluorescence compared with the well-researched visible and NIR-I (700-900 nm) window, providing a versatile platform for deep tissues/organs visualization with a greater

degree of clarity.[1-12] Whereas, the lack of highly bright fluorophores has become the bottleneck for progress in this area. Inorganic nanomaterials such as rare-earth nanoparticles,[13-14] carbon nanotubes,[15-16] quantum dots,[17-18] have been explored as excellent optical agents for NIR-II imaging. As alternatives, organic nanomaterials that are made from biologically inert components have the potential to avoid the toxicity concerns while having optical advantages equal or even better than inorganic counterparts.

Recently, semiconducting polymer nanoparticles (SPNs) composed of π-conjugated polymers have demonstrated as a versatile class of NIR absorbing/emitting biomaterials for fluorescence imaging, owing to their merits of good biocompatibility, excellent optical properties, high photostability, easy functionalization and potentially high biosafety.[19-28] SPNs normally consist of hydrophobic but optically tunable semiconducting polymers (SPs) and amphiphilic polymer matrix. Thereof, the molecular structure of SPs determines the optical properties of SPNs. As shown in Figure 1a, SPs are mainly designed as rigid planar π-conjugated structures, which possess excellent photophysical properties such as strong emission and absorption as isolated species. However, the emission of SPs is easily quenched in the aggregate state (aggregation-caused quenching, ACQ), owing to the dominated nonradiative decay induced by strong intermolecular π-π interactions.[29] To boost radiative decay, Tang *et al.* proposed a concept of aggregation-induced emission (AIE).[30-37] AIE luminogens (AIEgens) typically adopt twisted structures, which can significantly suppress the intermolecular interactions within nanoparticles (NPs), resulting in dramatically improved photoluminescence quantum yield (Φ_{PL}) (Figure 1b).[11, 38] Based on this strategy, Wu *et al.* reported NIR-II SPNs with a high Φ_{PL} of ~1.7%, assuring good quality for through-skull visualization of the cerebral vasculature in mice.[39] To achieve a high brightness, the absorption coefficient is also an important factor (equation 1).[40-43] However, considering the molecular design strategy of AIE, besides restricting intermolecular interactions, molecular distortion inevitably destroys the conjugation, giving an inferior absorption coefficient (Figure 1b). Thereof, increasing the absorption capacity of twisted structures may be a logical way to further boost the brightness of the fluorophores.

$$I_{PL} = \Phi_{PL} I_0 (1 - 10^{-A}) \qquad (1)$$

I_{PL} = photoluminescent emission intensity, I_0 = incident light intensity, A = absorbance,

Herein, we propose a molecular design strategy to enhance the brightness of NIR-II SPNs: structure planarization and twisting, combining the merits of high absorbance inherent from ACQ fluorophores and high Φ_{PL} originating from AIEgens. As shown in Figure 1c, by integration of planar structure (ACQ character) and twisted architecture (AIE-active) into one unit, the planar part assures the high absorption coefficient while the twisted part affords high Φ_{PL}. Thereof, the resulting SPNs can simultaneously display both high absorption coefficient and high Φ_{PL}. As a proof-of-concept, polymer pNIR-4 with partially planar and twisted structure displays a higher brightness with a high Φ_{PL} of 2.24% and molar extinction coefficient (ε) of 5.73×10^3 L mol^{-1} cm^{-1} than that of pNIR-1 (coplanar structure, Φ_{PL} = ~0, ε = 7.17×10^3 L mol^{-1} cm^{-1}) and pNIR-2 (twisted structure, Φ_{PL} = ~3.2%, ε = 3.26×10^3 L mol^{-1} cm^{-1}). Given that the brightness of dyes is determined by Φ_{PL} and absorption, quantum efficiency (QE) value is defined as QE = Φ_{PL} × ε to evaluate the brightness.[41] As expected, pNIR-4 NPs possess a superb QE (128) compared with pNIR-1 NPs (QE = ~0) and pNIR-2 NPs (QE = 104). Moreover, pNIR-4 NPs display emission maximum at 1040 nm with emission tail extending into the NIR-IIa region (1300-1400 nm), enabling in vivo NIR-IIa fluorescence image of blood vessels and lymph nodes. Moreover, a pH-responsive poly(β-amino ester) is adopted to enhance the accumulation of pNIR-4 in the tumor, realizing NIR-IIa fluorescence-guided cancer surgery. This study provides a molecular guideline to develop highly bright SPNs.

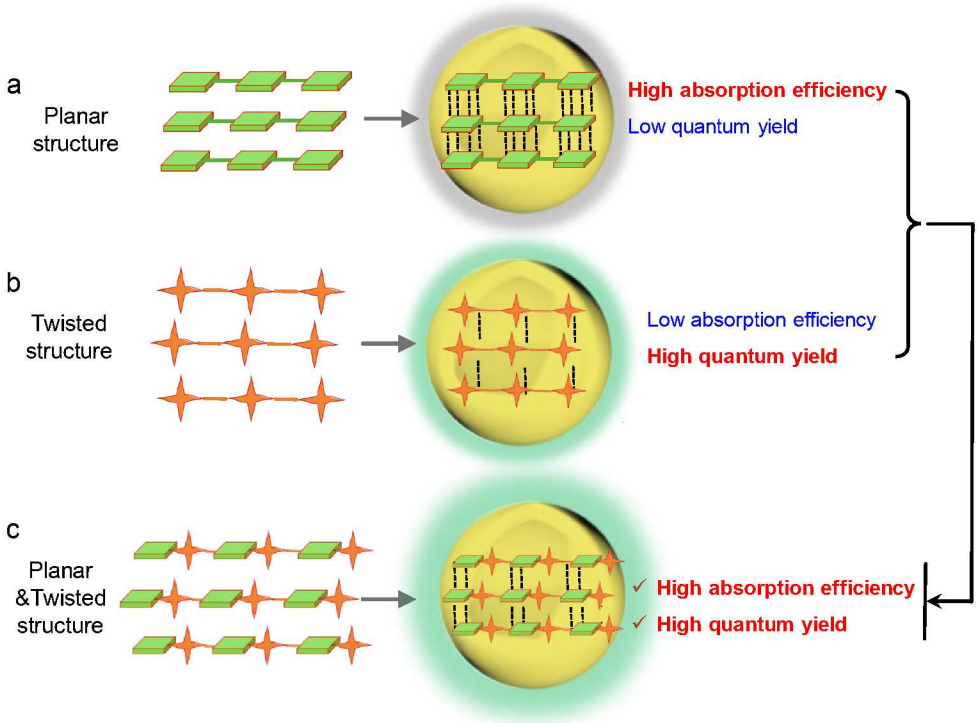

Figure 1. Schematic illustration of the molecular design philosophy of highly bright SPNs. (a) Planar structure. (b) Twisted structure. (c) Planar plus twisted structure.

Results and discussion

Design and Synthesis. First, molecular engineering approaches were carried out to construct SPs with strong emission in the NIR-II region. As shown in Figure 2, the SPs possessed a donor-acceptor (D-A) structure, with triphenylamine-based alkylthiophene (TAT) motif as D unit and benzo[1,2-c:4,5-c′]bis([1,2,5]thiadiazole) (BBTD) as A unit to give polymers a low bandgap.[44-45] Notably, we ingeniously manipulated the position of alkyl chains on the thiophene (T) to tune the configuration of the repeating units. For example, the *meta*-positioned alkyl units resulted in a coplanar T-BBTD-T structure because of steric distance between alkyl chains and BBTD core. While, *ortho*-positioned alkyl units gave rise to a twisted T-BBTD-T structure owing to the steric hindrance of the adjacent alkyl chains with BBTD core.[45-46] Triphenylamine (TPA) and tetraphenylethylene (TPE) acted as both molecular rotors to restrict the intermolecular interactions and molecular donors to drive the emission to the long-wavelength range. Thereof, polymer pNIR-1 featured with two *meta*-positioned hexyl units on the thiophene was synthesized (Figure 2a). The steric distance between the alkyl chain and BBTD core resulted in a coplanar structure, displaying excellent photophysical properties but might suffer from ACQ issues.[46] As a contrast, a polymer containing two *ortho*-positioned hexyl unit was defined as pNIR-2 (Figure 2b). The twisted structure caused by the steric hindrance between the alkyl chain and BBTD core was believed to suppress the intermolecular

π-π interactions to give an AIE character. To investigate the donor effect, polymer pNIR-3 decorated with a weaker TPE unit was also designed (Figure 2c). To manifest the molecular design philosophy, pNIR-4 with *meta*- and *ortho*-positioned hexyl unit was synthesized (Figure 2d). The key structural feature of pNIR-4 was the integration of planar and twisted block into one molecule. On the one hand, the planar motif could enhance the absorptivity due to a better conjugation. On the other hand, the twisted unit could afford a high Φ_{PL} in aggregate via restriction of intermolecular interactions. Therefore, improved brightness might be achieved by enhancing Φ_{PL} and absorption simultaneously. The intermediates and products were characterized by NMR and gel permeation chromatography methods (Supporting Information).

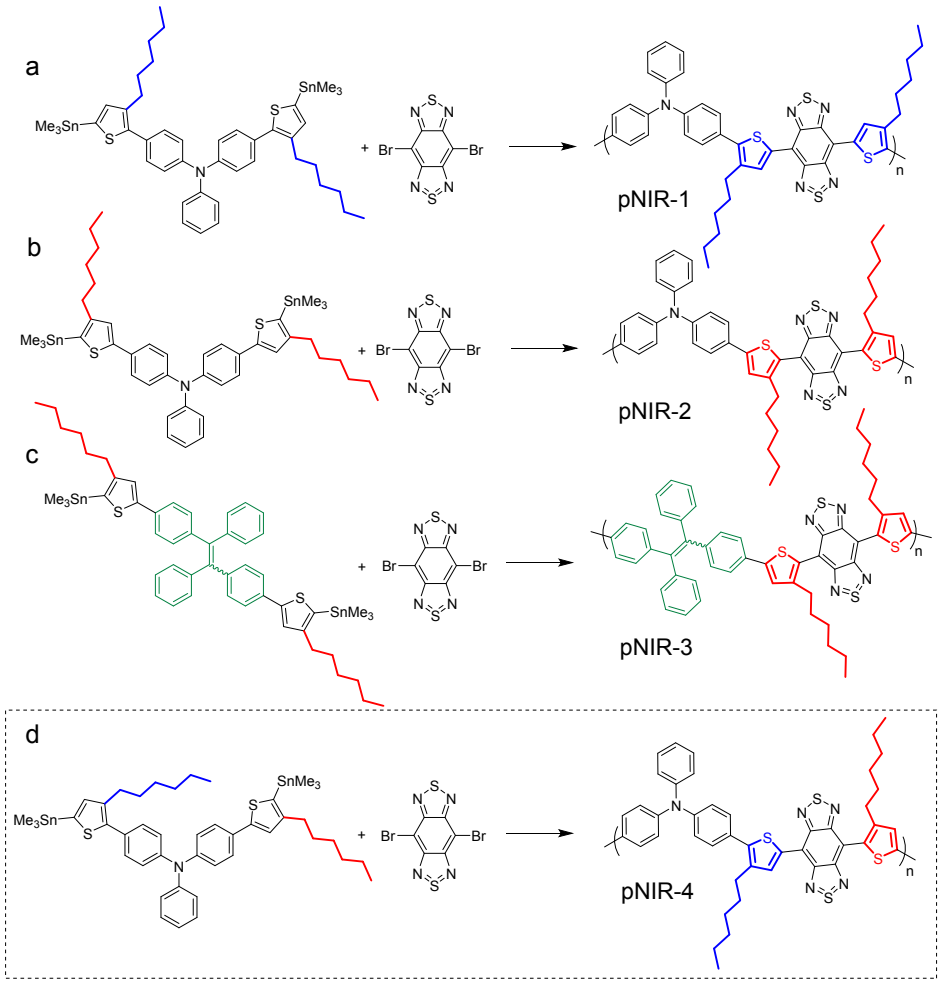

Figure 2. Synthetic routes to conjugated polymers. (a) pNIR-1. (b) pNIR-2. (c) pNIR-3. (d) pNIR-4.

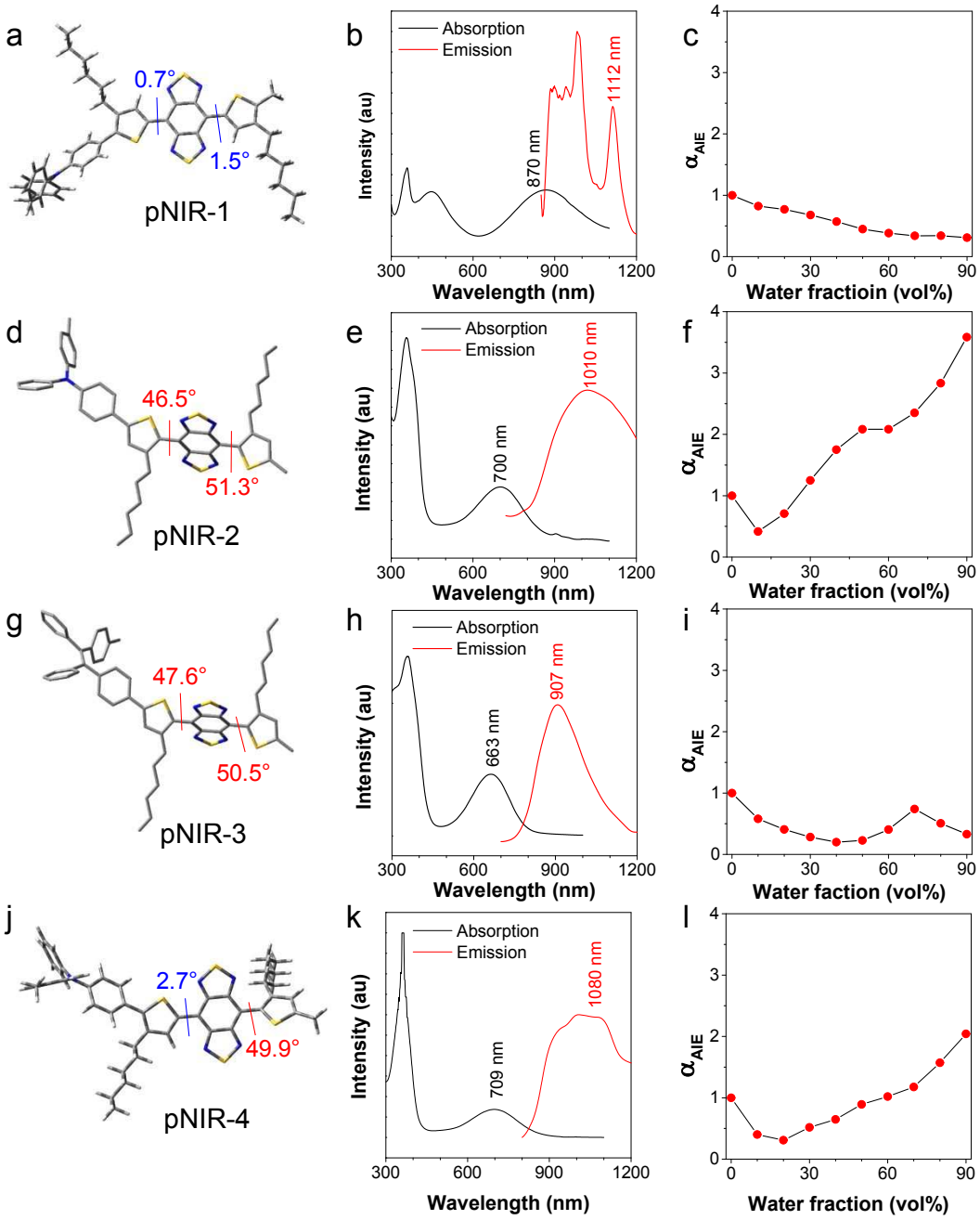

Figure 3. Theoretical calculation results of polymer pNIR-1, pNIR-2, pNIR-3, pNIR-4 and their respective optical spectra. (a, d, g, j) Optimized ground-state geometries. (b, e, h, k) Absorption and emission spectra in THF. (c, f, i, l) PL intensity variation with water fraction in THF/H_2O mixtures.

To assess the geometry of the polymers, density functional theory (DFT) calculations in the gaseous state were performed. In pNIR-1, the dihedral angles of BBTD and thiophene at the optimized ground-state (S_0) were only 0.7° and 1.5°, respectively (Figure 3a, S1), suggesting a coplanar structure that resulted from the steric distance between *meta*-positioned alkyl chain and BBTD core.[46] Thanks to this planar structure,

pNIR-1 possessed a high ε of 7.17×10^3 L mol^{-1} cm^{-1} at 870 nm, while the emission peak located at ~1112 nm (Figure 3b, S2). As expected, pNIR-1 showed obvious ACQ effect with a Φ_{PL} of ~ 0 in nanoparticles. This result indicated that the presence of twisted TPA unit could hardly restrict the predominated inter/intramolecular interactions (Figure 3c, S3). It is for this reason that planar conjugated polymers find wide applications in photothermal therapy or photoacoustic imaging.[47-48] In pNIR-2, the *ortho*-positioned hexyl unit significantly distorted the backbone, as reflected from the a large dihedral degree of 46.5° and 53.5° (Figure 3d). The backbone distortion broke the conjugation resulting in blue-shifted absorption (700 nm) and emission (1010 nm) (Figure 3e). To our delight, the pNIR-2 showed a typical AIE character with the PL intensity increasing with water fraction, giving an α_{AIE} (PL intensity ratio of 90% water fraction to that of pure THF) = 3.6 (Figure 3f). Notably, pNIR-2 displayed a Φ_{PL} of 3.2% (Figure S4,5), which is higher than previous reports (Table S1),[42, 49-50] owing to the efficient hindrance of inter/intramolecular interactions. However, the twisted architecture damaged the absorption coefficient, giving a low ε of 3.26×10^3 L mol^{-1} cm^{-1} at 700 nm.[43] The quantum efficiency value QE was only 104. On the other hand, by changing the molecular rotor from the triphenylamine (TPA) unit to TPE, polymer pNIR-3 still adopted a twisted backbone (dihedral degree of 47.6° and 50.5°) (Figure 3g). The absorption and emission peak of polymer pNIR-3 blue-shifted to 663 and 907 nm, respectively, owing to the weaker electron-donating ability of TPE (Figure 3h). Nevertheless, pNIR-3 displayed part of ACQ character with an α_{AIE} of 0.3, possibly owing to the active intramolecular motion of TPE units within NPs (Figure 3i).[32] Polymer pNIR-3 had a high ε of 1.06×10^4 L mol^{-1} cm^{-1} at 663 nm with a fluorescent Φ_{PL} of 1.9%. Despite a relatively high QE (201), the fluorescent emission was mainly in the NIR-I range (700-950 nm), which might encounter light scattering and attenuation with improved imaging depth.[2] In polymer pNIR-4, the distinct dihedral angles of 2.7° and 49.9° demonstrated that the backbone adopted a planar plus twisted structure (Figure 3j). Compared to complete twisting pNIR-2, polymer pNIR-4 showed a redshift in both absorption (709 nm) and emission (broad peak: 1012~1080 nm) (Figure 3k). pNIR-4 possessed an enhanced ε of 5.73×10^3 L mol^{-1} cm^{-1} at 709 nm with a high Φ_{PL} of 2.24%. Notably, the QE of pNIR-4 reached up to 128, much higher than the complete twisting counterpart pNIR-3 (QE = 105), demonstrating the feasibility of the present molecular design strategy. The PL intensity of pNIR-4 decreased first and then increased with the increase of water fraction (Figure 3l). The decreased PL intensity with water addition was due to the formation of twisted intramolecular charge transfer (TICT) state, whose predominated nonradiative decay quenched the emission.[51] Further increase of water fraction triggered the AIE mechanism via restriction of intramolecular motions, giving an α_{AIE} of 2.0. The photophysical properties of above conjugated polymers are summarized in Table S2. Overall, enhanced brightness can be obtained by integration planar and twisted structure into one polymer.

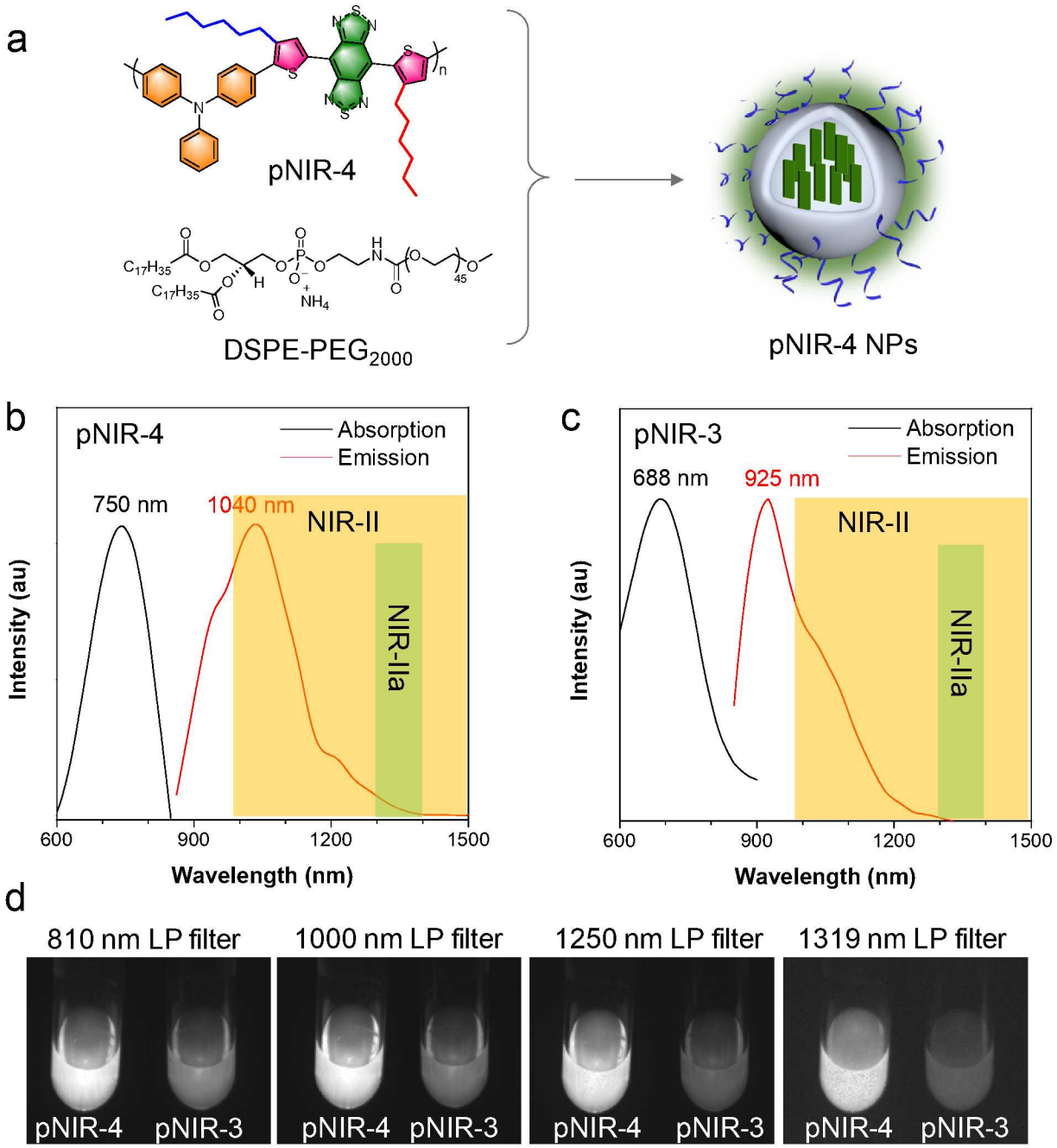

Figure 4. (a) Schematic illustration of the fabrication of pNIR-4 NPs. Absorption and emission spectra of (b) pNIR-4 and (c) pNIR-3 NPs. (d) Comparison of NIR signal of pNIR-3 and pNIR-4 NPs under various LP filters (810-1319 nm) (808 nm excitation, 20 mW/cm^2).

Fluorescence imaging in the NIR-IIa (1300-1400) window outperformed conventional NIR-II imaging with enhanced signal-to-background ratio (SBR), high resolution and increased image clarity because of further suppressed photon scattering.[52-54] Based on the outstanding brightness of pNIR-4, we investigated

the in vitro fluorescence imaging. To endow excellent water dispersity, pNIR-4 was formulated into NPs through the nanoprecipitation method by the assistance of amphiphilic polymer DSPE-PEG_{2000} (Figure 4a). The dynamic light scattering and transmission electron microscopy results suggested a hydrodynamic diameter of ~100 nm for spherical pNIR-4 NPs (Figure S6). The pNIR-4 NPs showed a typical NIR-I absorption at 750 nm with a tail extending to 900 nm, which could penetrate much deeper tissues and trigger less photodamage (Figure 4b). On the other hand, the emission profile of pNIR-4 NPs was maximized at ~1040 nm, with an obvious tail stretching to 1400 nm, which showed potential for NIR-IIa bioimaging. To demonstrate the advantages of NIR-IIa imaging, pNIR-3 NPs with NIR-I emission (925 nm) and negligible fluorescence signal after 1300 nm were used as a control (Figure 4c). As shown in Figure 4d, the pNIR-4 NPs were significantly brighter than pNIR-3 NPs under different long-pass (LP) filters of -810, -1000, -1250 and -1319 nm, again suggesting the success of present molecular design strategy. In addition, a linear enhancement in fluorescent intensity with concentrations was observed from the NIR-IIa signal of pNIR-4 NPs (Figure S7), providing a platform for quantitative analysis. Moreover, pNIR-4 NPs displayed excellent photostability, which was of vital importance for practical applications (Figure S8).

To investigate the feasibility of pNIR-4 NPs as NIR-IIa probe in vivo, the images of the mouse brain and hindlimb vasculatures were monitored by intravenous injection (Figure 5a). In contrast to sharper and higher resolution images detected in the NIR-IIa region (1319 nm LP), the vasculatures looked blurry in the NIR-II region (1000 nm LP), demonstrating the merit of NIR-IIa imaging. It should be noted that pNIR-4 NPs cannot penetrate the blood-brain-barrier according to their tissue distribution (Figure S9). NIR-IIa imaging with pNIR-3 NPs provided the information of main vessels that were hard to discern (Figure 5b). In contrast, detailed small capillaries could be seen by pNIR-4 NPs in the NIR-IIa region with high clarity, reflecting its high brightness (Figure 5b). The signal is visible in vitro even at the depth of 9 mm (Figure S10). All these results demonstrated that pNIR-4 NPs were suitable for NIR-IIa imaging and outperformed traditional NIR-II imaging.

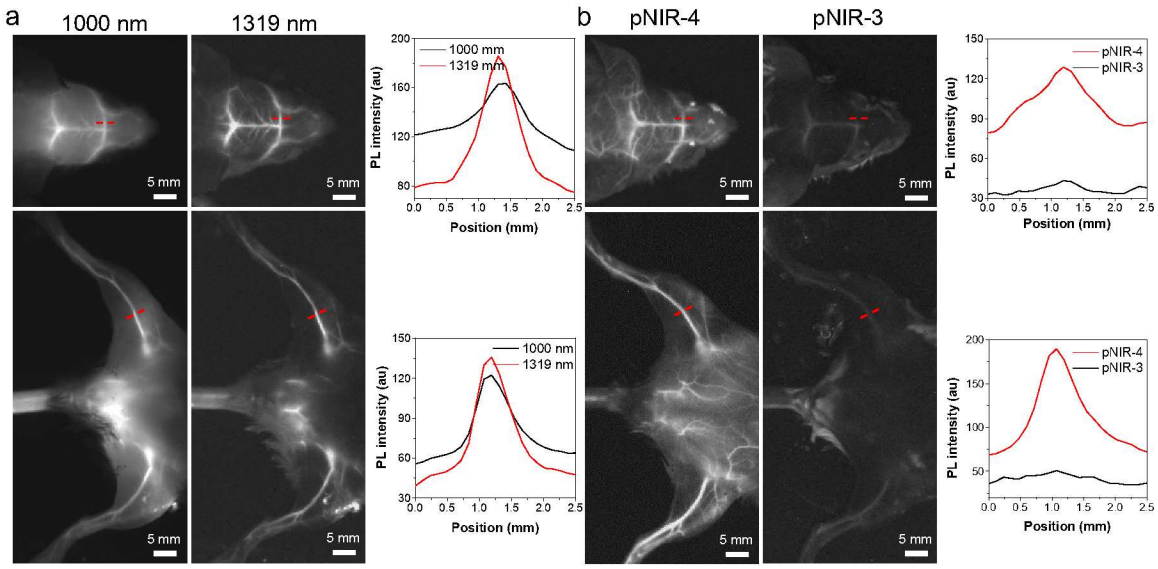

Figure 5. (a) NIR-II fluorescent imaging of blood vessels in cerebral cortex and hindlimb under different LP filters, respectively, and their corresponding cross-sectional intensity profile along the red-dashed lines. At 2 minutes post-injection of pNIR-4 NPs via tail vein, the mice were euthanatized and imaged under 1000 and 1319 nm LP filter, respectively. (b) Comparison of NIR-IIa fluorescent imaging quality between pNIR-4 and pNIR-3 nanoparticles, and their corresponding cross-sectional intensity profile along the red-dashed lines. The mice were imaged under 1319 nm LP filter at 5 minutes post-injection of pNIR-4 and pNIR-3 NPs, respectively.

In clinical surgical oncology, intraoperative imaging had a considerable role in promoting the surgery outcomes via precise discrimination and resection of tumor nodules.[55-56] Although magnetic resonance imaging and computed tomography played a great role in guiding intraoperative resection plans, the complex operation, expensive cost and harmful ionizing radiation made them improper for surgical procedure. NIR-II fluorescence imaging is a promising technique to identify tumor margins with high sensitivity in virtue of its improved SBR, whose precise image-guided intraoperative tumor-removal surgery in deep tissue has been demonstrated by several reports.[57-60] However, the NIR-IIa imaging-guided intraoperative tumor-removal surgery by SPNs have not been developed. Notably, in addition to fluorescence emission efficiency, the accumulation of fluorescence probes in the tumor site played an equally important role. However, during the delivery of NPs to tumor sites, there is often a contradiction between the blood circulation time and tumor cell uptake efficiency. Thereof, to overcome this dilemma for enhanced tumor retention, a pH-responsive copolymer PCL-*b*-PAE and a commonly used polymer with long blood circulation time, PCL-*b*-PEG, were used as the mixed matrix to encapsulate pNIR-4, forming surface-adaptive pNIR4-PAE NPs (Figure 6a).[61] In the blood, pNIR4-PAE NPs with only PEG-exposed surfaces exhibited long blood circulation time. While in the acidic tumor microenvironment (pH = 6.5-6.8), the PAE was protonated, leading to the stretch and exposure of positively-charged PAE on the surfaces of pNIR4-PAE NPs. Such positively-charged surfaces could enhance the accumulation and cellular uptake of

pNIR4-PAE NPs at tumor sites (Figure S11).[62] To confirm the pH-responsiveness of pNIR4-PAE NPs, pNIR-4 encapsulated by PCL-*b*-PEG (pNIR4-PEG NPs) was used as control. The pNIR4-PAE NPs displayed a hydrodynamic diameter of ~120 nm with high colloidal stability, slightly larger than that of pNIR4-PEG NPs (110 nm) (Figure S12-14). As shown in Figure S15, the charge of pNIR4-PAE NPs switched into positive when the pH is below 6.8, which will facilitate their internalization by tumor cells. In contrast, the zeta potential of pNIR4-PEG NPs kept negative under a pH of 5.0-7.4. To monitor the internalization efficiency, cy5-labelled PCL-*b*-PEG was utilized as part of the structural material because it can be visualized by a confocal microscope. After a 2 h incubation with PEG NPs and PAE NPs at pH 7.4 and 6.5, respectively, a brightest red signal was detected in the HepG2 cells incubated with PAE NPs under pH 6.5, which was also confirmed by the flow cytometry (Figure S16). This result suggested the positively-charged NPs at pH = 6.5 will strengthen their interaction with tumor cells and enhance tumor cellular internalization. Encouragingly, pNIR4-PAE NPs displayed an obvious tumor-targeting ability than that of pNIR4-PEG NPs in subcutaneous tumor-bearing mice (Figure S17). Therefore, the pNIR4-PAE NPs that can be activated to be positively charged in tumor microenvironment were internalized efficiently by tumor cells both in vitro and in vivo, which is beneficial for precisely tumor imaging.

Peritoneal carcinomatosis is usually related with a low overall survival rate and its preoperative assessment and intraoperative imaging are very challenging due to the dispersion of large amounts of tumor nodules with diameters <1 mm scattered in the peritoneal cavity.[63-64] These tiny tumor nodules that are hard to be spotted are the major reasons for the cancer recurrence. Thus, we established peritoneal carcinomatosis-bearing mice to assess whether pNIR4-PAE NPs can assist the surgical discrimination and resection of ultrasmall tumor nodules. To better monitor the tumor distribution, luciferase-expressed 4T1 tumors were selected which exhibited bioluminescence upon postinjection with D-luciferin. After 24h intravenously injection of pNIR4-PAE NPs, the NIR-IIa fluorescence of pNIR4-PAE NPs and the bioluminescence signal of luciferase are colocalized perfectly in the peritoneal cavity (Figure 6b), demonstrating the accurate tumor diagnosis of pNIR4-PAE NPs. In the clinic, the surgeon always relied on naked eyes and hands to determine which tissues need to be removed or to be preserved. Although relatively large diameters (>1 mm) tumors have been removed by the surgeon (Tianjin First Central Hospital) under unguided surgery, many small tumor nodules remained, which was difficult to be identified. Followed by a second-round operation guided by NIR-IIa fluorescence, reduction of tumor burden was observed. The bioluminescence signals of all the harvested tumor nodules verified the resected tissue was indeed a tumor, proving the precise cancer surgery with the help of pNIR4-PAE NPs (Figure 6c). By quantifying the diameters of excised tumor nodules, more submillimeter tumors have been excised assisted by intraoperative imaging (Figure 6d). These results suggested that the cancer surgery outcome could be

promoted by accurately identification of submillimeter tumor nodules with pNIR4-PAE NPs, largely reducing the risk of in situ tumor recurrence.

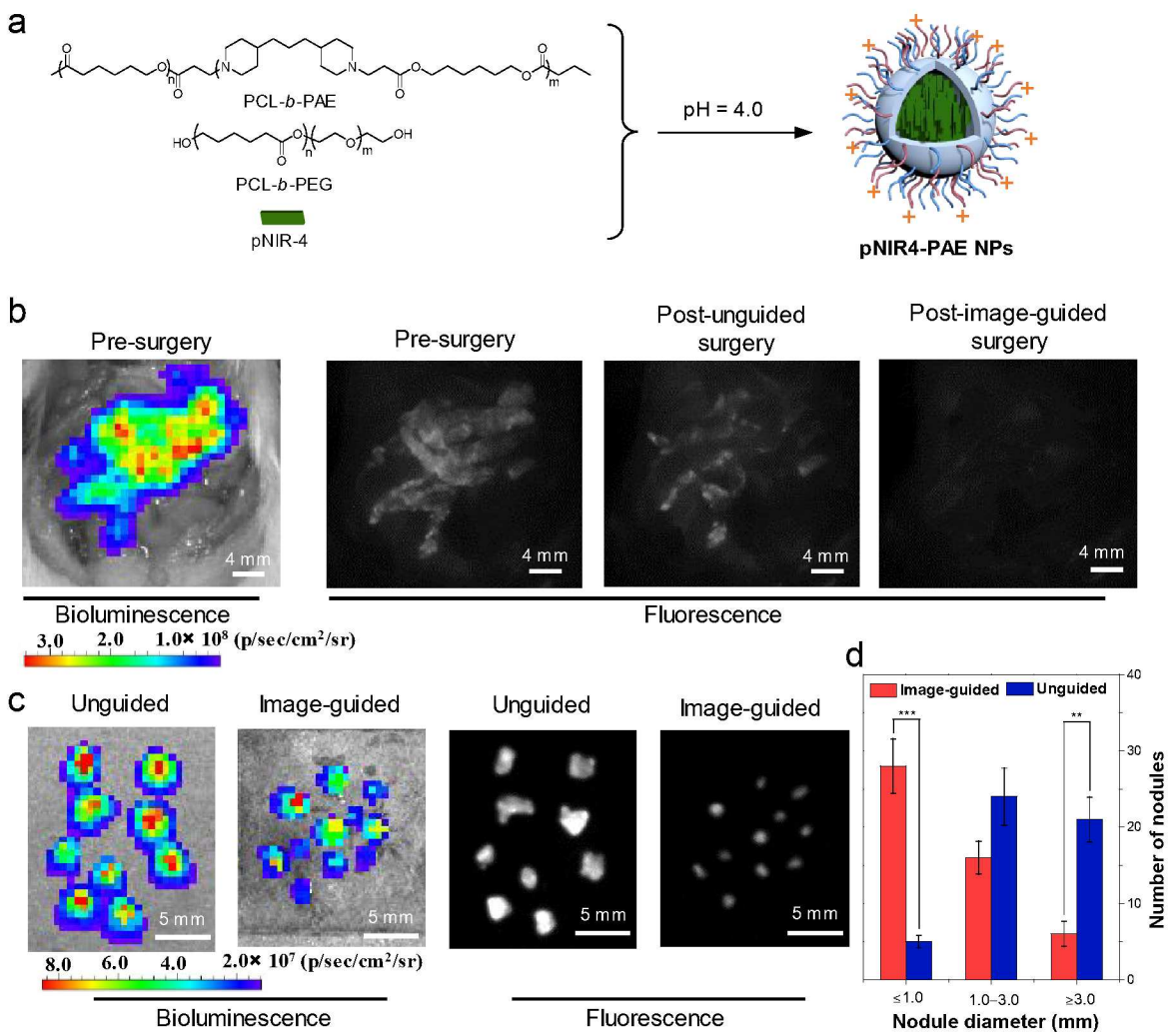

Figure 6. Tumor resection with and without pNIR4-PAE NPs image-guided surgery. (a) Schematic illustration of the fabrication of pNIR4-PAE NPs. (b) Bioluminescence and NIR- IIa imaging of the abdominal cavity before and after tumor resection. (c) Bioluminescence and NIR-IIa imaging of resected nodules of unguided and pNIR4-PAE NPs guided groups. (d) Statistical data of nodules diameters resected (*P < 0.05, **P < 0.01, ***P < 0.001, n=3).

Hundreds of thousands of patients have been affected by cancer metastasis yearly through the lymphatic system, so it is highly important to identify and dissect their lymphatic system.[65-69] To assess the potential clinical utility of pNIR-4 NPs for lymphography, a ~50 μL solution (1 mg/mL) of pNIR-4 NPs was subcutaneously injected into the footpads of nude mice. Immediately after injection, pNIR-4 NPs migrated into the lymphatic vasculature deviated from the injection site and the sentinel lymph node (SLN) was observed (Figure 7a). Moreover, the lymphatic duct between two lymph nodes could be visualized at 60 s

post-injection of pNIR-4 NPs. To again illustrate the advantages of NIR-IIa imaging, the same dose of pNIR-3 NPs was injected in the footpad as well, while the vessel anatomy and lymph nodes looked ambiguous (Figure 7b, S18). Owing to the less photons scattering in the NIR-IIa region, pNIR-4 NPs provided clearer visual guidance to surgeons for minimizing inaccuracies in incision and dissection. To verify the accumulation of pNIR-4 NPs in the SLN, the lymphatic counterstain methylene blue was reinjected at the same site, with its blue color well colocalized with the fluorescence of pNIR-4 NPs (Figure 7c, d). Moreover, with the guidance of the NIR-IIa fluorescence signal of pNIR-4 NPs, the SLN with a smallest diameter of ~1 mm were precisely removed (Figure 7e). Notably, pNIR-4 NPs and pNIR4-PAE NPs displayed good cytocompatibility and in vivo biocompatibility (Figure S19-21). Overall, pNIR-4 SPNs enabled as a new and stable NIR-IIa probe for intraoperative imaging, including cancer resection and lymph nodes dissection, which provides strong technical support for surgical navigation in the clinic.

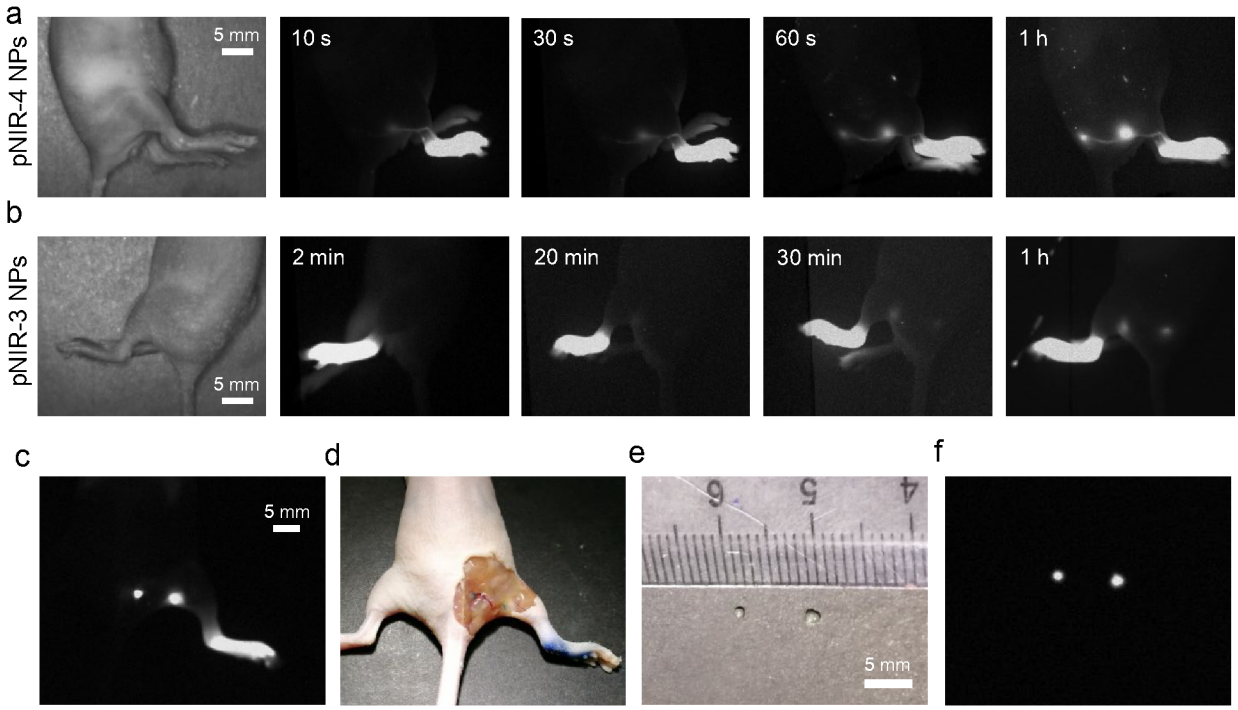

Figure 7. In vivo NIR-II fluorescence imaging of the lymphatic system with pNIR-4 and pNIR-3 NPs, respectively. (a) Bright field and fluorescence field of live mice by subcutaneous injection of (a) pNIR-4 NPs and (b) pNIR-3 NPs (50 μL, 1mg/mL). Note, fluorescent images were captured at different time. (c) NIR-IIa fluorescence images of the mouse injected intradermally with pNIR4 NPs in the right paw. (d) Color image of the mouse after reinjection with 20 μL of 1% methylene blue. Color (e) and NIR-IIa fluorescence (f) images of SLN extracted from the mouse under NIR-IIa fluorescence guidance after injection with pNIR4 NPs.

Conclusions

In summary, we have developed a molecular design philosophy of "integration of planar and twisted blocks into one molecule" to boost the brightness of SPNs. ACQ fluorophores typically adopt a planar π-

conjugated structure displaying strong absorptivity but suffer from fluorescence quenching in the aggregate state. On the other hand, AIEgens have twisted backbones showing high solid-state Φ_{PL} at the cost of absorptivity. The key point of the present strategy lies in getting essence from the merits of these two types of conflicting molecules: ACQ fluorophores and AIEgens. We utilized the steric hindrance produced by the adjacent alkylthiophene unit to tune the configuration of the polymer repeating units. The *ortho*-positioned alkyl chains give twisted structure while the *meta*-positioned one results in a coplanar structure, which is demonstrated by DFT calculations. The resultant polymer pNIR-4 with planar plus twisted structure shows Φ_{PL} of 2.24% and ε of 5.73×10^3 L mol^{-1} cm^{-1} at 709 nm. Polymer pNIR-1 with planar structure displays Φ_{PL} of ~0 and ε of 7.17×10^3 L mol^{-1} cm^{-1} at 870 nm. Polymer pNIR-2 with twisted structure exhibits Φ_{PL} of ~3.2 and ε of 3.26×10^3 L mol^{-1} cm^{-1} at 870 nm. Since brightness is the product of Φ_{PL} and ε, pNIR-4 possesses superb brightness (QE = 128) than that of planar pNIR-1 (QE = ~0) and twisted pNIR-2 (QE = 104). Given the emission tail extending into the NIR-IIa region (1300-1400 nm) of bright p-NIR4 NPs, NIR-IIa fluorescence imaging of blood vessels with enhanced clarity is observed. Moreover, a pH-responsive PAE polymer makes p-NIR4 NPs specifically accumulate at tumor sites, allowing NIR-IIa fluorescence image-guided cancer resection. The present study demonstrates the tuning of molecular structure to boost the brightness of fluorophores and will inspire the development of highly bright fluorescent dyes.

Associated Content

Supporting Information. General information about materials and methods, synthesis and characterizations, NMR spectra of the compounds.

Author Information

Corresponding Author

*E-mail: dingd@nankai.edu.cn.

*E-mail: tangbenz@ust.hk.

ORCID

Shunjie Liu: 0000-0003-1632-0183

Dan Ding: 0000-0003-1873-6510

Ben Zhong Tang: 0000-0002-0293-964X

Author Contributions

[#]S. L. and H. O. contributed equally to this work.

Notes

The authors declare no competing financial interest.

Acknowledgment

The project was financially supported by National Natural Science Foundation of China (51961160730, 51873092, 21788102 and 21805002), the Research Grants Council of Hong Kong (AHKUST605/16 and C6009-17G), the Innovation and Technology Commission (ITCCNERC14SC01 and ITCPD/17-9), the Science and Technology Plan of Shenzhen (JCYJ20180507183832744), the Ming Wai Lau Centre for Reparative Medicine Associate Member Programme, the National Key R&D Program of China (Intergovernmental cooperation project, 2017YFE0132200), and the Fundamental Research Funds for the Central Universities, Nankai University.

Reference

1. Miao, Y.; Gu, C.; Zhu, Y.; Yu, B.; Shen, Y.; Cong, H., Recent Progress in Fluorescence Imaging of the Near-Infrared II Window. *ChemBioChem* **2018,** *19* (24), 2522-2541.
2. Zhu, S.; Tian, R.; Antaris, A. L.; Chen, X.; Dai, H., Near-Infrared-II Molecular Dyes for Cancer Imaging and Surgery. *Adv. Mater.* **2019,** *31* (24), 1900321.
3. Tang, Y.; Pei, F.; Lu, X.; Fan, Q.; Huang, W., Recent Advances on Activatable NIR-II Fluorescence Probes for Biomedical Imaging. *Adv. Opt. Mater.* **2019,** *7* (21), 1900917.
4. Li, C.; Wang, Q., Advanced NIR-II Fluorescence Imaging Technology for In Vivo Precision Tumor Theranostics. *Adv. Ther.* **2019,** *2* (9), 1900053.
5. Hong, G.; Diao, S.; Antaris, A. L.; Dai, H., Carbon nanomaterials for biological imaging and nanomedicinal therapy. *Chem. Rev.* **2015,** *115* (19), 10816-10906.
6. Xu, S.; Cui, J.; Wang, L., Recent developments of low-toxicity NIR II quantum dots for sensing and bioimaging. *TrAC, Trends Anal. Chem.* **2016,** *80*, 149-155.
7. Naczynski, D. J.; Tan, M. C.; Riman, R. E.; Moghe, P. V., Rare earth nanoprobes for functional biomolecular imaging and theranostics. *J. Mater. Chem. B* **2014,** *2* (20), 2958-2973.
8. Cao, J.; Zhu, B.; Zheng, K.; He, S.; Meng, L.; Song, J.; Yang, H., Recent Progress in NIR-II Contrast Agent for Biological Imaging. *Front Bioeng Biotechnol.* **2020,** *7*, 487-487.
9. Kenry; Duan, Y.; Liu, B., Recent Advances of Optical Imaging in the Second Near-Infrared Window. *Adv. Mater.* **2018,** *30* (47), 1802394.
10. Ding, F.; Fan, Y.; Sun, Y.; Zhang, F., Beyond 1000 nm Emission Wavelength: Recent Advances in Organic and Inorganic Emitters for Deep-Tissue Molecular Imaging. *Adv. Healthc. Mater.* **2019,** *8* (14), 1900260.
11. Liu, S.; Li, Y.; Kwok, R. T. K.; Lam, J. W. Y.; Tang, B. Z., Structural and process controls of AIEgens for NIR-II theranostics. *Chem. Sci.* **2020**, DOI: 10.1039/d0sc02911d.
12. Xu, W.; Wang, D.; Tang, B. Z., NIR-II AIEgens: A Win-Win Integration towards Bioapplications. *Angew. Chem. Int. Ed.* 10.1002/anie.202005899.
13. Wang, R.; Zhou, L.; Wang, W.; Li, X.; Zhang, F., In vivo gastrointestinal drug-release monitoring through second near-infrared window fluorescent bioimaging with orally delivered microcarriers. *Nat. Commun.* **2017,** *8* (1), 1-12.

14. Naczynski, D. J.; Tan, M. C.; Zevon, M.; Wall, B.; Kohl, J.; Kulesa, A.; Chen, S.; Roth, C. M.; Riman, R. E.; Moghe, P. V., Rare-earth-doped biological composites as in vivo shortwave infrared reporters. *Nat. Commun.* **2013,** *4* (1), 2199.
15. Antaris, A. L.; Robinson, J. T.; Yaghi, O. K.; Hong, G.; Diao, S.; Luong, R.; Dai, H., Ultra-low doses of chirality sorted (6, 5) carbon nanotubes for simultaneous tumor imaging and photothermal therapy. *ACS Nano* **2013,** *7* (4), 3644-3652.
16. Dang, X.; Gu, L.; Qi, J.; Correa, S.; Zhang, G.; Belcher, A. M.; Hammond, P. T., Layer-by-layer assembled fluorescent probes in the second near-infrared window for systemic delivery and detection of ovarian cancer. *Proc. Natl. Acad. Sci. U.S.A.* **2016,** *113* (19), 5179-5184.
17. Franke, D.; Harris, D. K.; Chen, O.; Bruns, O. T.; Carr, J. A.; Wilson, M. W.; Bawendi, M. G., Continuous injection synthesis of indium arsenide quantum dots emissive in the short-wavelength infrared. *Nat. Commun.* **2016,** *7*, 12749.
18. Li, C.; Li, F.; Zhang, Y.; Zhang, W.; Zhang, X.-E.; Wang, Q., Real-time monitoring surface chemistry-dependent in vivo behaviors of protein nanocages via encapsulating an NIR-II Ag2S quantum dot. *ACS Nano* **2015,** *9* (12), 12255-12263.
19. Jiang, Y. Y.; Pu, K. Y., Multimodal Biophotonics of Semiconducting Polymer Nanoparticles. *Acc. Chem. Res.* **2018,** *51* (8), 1840-1849.
20. Tuncel, D.; Demir, H. V., Conjugated polymer nanoparticles. *Nanoscale* **2010,** *2* (4), 484-494.
21. Li, K.; Liu, B., Polymer encapsulated conjugated polymer nanoparticles for fluorescence bioimaging. *J. Mater. Chem.* **2012,** *22* (4), 1257-1264.
22. Feng, L.; Zhu, C.; Yuan, H.; Liu, L.; Lv, F.; Wang, S., Conjugated polymer nanoparticles: preparation, properties, functionalization and biological applications. *Chem. Soc. Rev.* **2013,** *42* (16), 6620-6633.
23. Li, J.; Rao, J.; Pu, K., Recent progress on semiconducting polymer nanoparticles for molecular imaging and cancer phototherapy. *Biomaterials* **2018,** *155*, 217-235.
24. Wu, C.; Chiu, D. T., Highly Fluorescent Semiconducting Polymer Dots for Biology and Medicine. *Angew. Chem. Int. Ed.* **2013,** *52* (11), 3086-3109.
25. Yu, J.; Rong, Y.; Kuo, C.-T.; Zhou, X.-H.; Chiu, D. T., Recent advances in the development of highly luminescent semiconducting polymer dots and nanoparticles for biological imaging and medicine. *Anal. Chem.* **2017,** *89* (1), 42-56.
26. Huang, J.; Xie, C.; Zhang, X.; Jiang, Y.; Li, J.; Fan, Q.; Pu, K., Renal-clearable Molecular Semiconductor for Second Near-Infrared Fluorescence Imaging of Kidney Dysfunction. *Angew. Chem. Int. Ed.* **2019,** *58* (42), 15120-15127.
27. Huang, J.; Pu, K., Activatable Molecular Probes for Second Near-Infrared Fluorescence, Chemiluminescence, and Photoacoustic Imaging. *Angew. Chem. Int. Ed.* **2020,** *59* (29), 11717-11731.
28. Miao, Q.; Xie, C.; Zhen, X.; Lyu, Y.; Duan, H.; Liu, X.; Jokerst, J. V.; Pu, K., Molecular afterglow imaging with bright, biodegradable polymer nanoparticles. *Nat. Biotechnol.* **2017,** *35* (11), 1102.
29. Pu, K.; Mei, J.; Jokerst, J. V.; Hong, G.; Antaris, A. L.; Chattopadhyay, N.; Shuhendler, A. J.; Kurosawa, T.; Zhou, Y.; Gambhir, S. S., Diketopyrrolopyrrole-based semiconducting polymer nanoparticles for in vivo photoacoustic imaging. *Adv. Mater.* **2015,** *27* (35), 5184-5190.
30. Zhang, H.; Zhao, Z.; McGonigal, P. R.; Ye, R.; Liu, S.; Lam, J. W. Y.; Kwok, R. T. K.; Yuan, W. Z.; Xie, J.; Rogach, A. L.; Tang, B. Z., Clusterization-triggered emission: Uncommon luminescence from common materials. *Mater. Today* **2020,** *32*, 275-292.
31. Mei, J.; Leung, N. L. C.; Kwok, R. T. K.; Lam, J. W. Y.; Tang, B. Z., Aggregation-Induced Emission: Together We Shine, United We Soar! *Chem. Rev.* **2015,** *115* (21), 11718-11940.
32. Liu, S.; Li, Y.; Zhang, H.; Zhao, Z.; Lu, X.; Lam, J. W. Y.; Tang, B. Z., Molecular Motion in the Solid State. *ACS Materials Lett.* **2019,** *1* (4), 425-431.
33. Li, Y.; Liu, S.; Han, T.; Zhang, H.; Chuah, C.; Kwok, R. T. K.; Lam, J. W. Y.; Tang, B. Z., Sparks fly when AIE meets with polymers. *Mater. Chem. Front.* **2019,** *3* (11), 2207-2220.
34. Cheng, H.-B.; Li, Y.; Tang, B. Z.; Yoon, J., Assembly strategies of organic-based imaging agents for fluorescence and photoacoustic bioimaging applications. *Chem. Soc. Rev.* **2020,** *49* (1), 21-31.

35. Ding, D.; Li, K.; Liu, B.; Tang, B. Z., Bioprobes Based on AIE Fluorogens. *Acc. Chem. Res.* **2013,** *46* (11), 2441-2453.
36. Hu, F.; Xu, S.; Liu, B., Photosensitizers with Aggregation-Induced Emission: Materials and Biomedical Applications. *Adv. Mater.* **2018,** *30* (45), 1801350.
37. Liu, S.; Zhang, H.; Li, Y.; Liu, J.; Du, L.; Chen, M.; Kwok, R. T. K.; Lam, J. W. Y.; Phillips, D. L.; Tang, B. Z., Strategies to Enhance the Photosensitization: Polymerization and the Donor–Acceptor Even–Odd Effect. *Angew. Chem. Int. Ed.* **2018,** *57* (46), 15189-15193.
38. Liu, S.; Cheng, Y.; Li, Y.; Chen, M.; Lam, J. W. Y.; Tang, B. Z., Manipulating Solid-State Intramolecular Motion toward Controlled Fluorescence Patterns. *ACS Nano* **2020,** *14* (2), 2090-2098.
39. Zhang, Z.; Fang, X.; Liu, Z.; Liu, H.; Chen, D.; He, S.; Zheng, J.; Yang, B.; Qin, W.; Zhang, X.; Wu, C., Semiconducting Polymer Dots with Dual-Enhanced NIR-IIa Fluorescence for Through-Skull Mouse-Brain Imaging. *Angew. Chem. Int. Ed.* **2020,** *59* (9), 3691-3698.
40. Piwoński, H.; Li, W.; Wang, Y.; Michinobu, T.; Habuchi, S., Improved Fluorescence and Brightness of Near-Infrared and Shortwave Infrared Emitting Polymer Dots for Bioimaging Applications. *ACS Appl. Polym. Mater.* **2020,** *2* (2), 569-577.
41. Zhu, S.; Hu, Z.; Tian, R.; Yung, B. C.; Yang, Q.; Zhao, S.; Kiesewetter, D. O.; Niu, G.; Sun, H.; Antaris, A. L.; Chen, X., Repurposing Cyanine NIR-I Dyes Accelerates Clinical Translation of Near-Infrared-II (NIR-II) Bioimaging. *Adv. Mater.* **2018,** *30* (34), 1802546.
42. Hong, G. S.; Zou, Y. P.; Antaris, A. L.; Diao, S.; Wu, D.; Cheng, K.; Zhang, X. D.; Chen, C. X.; Liu, B.; He, Y. H.; Wu, J. Z.; Yuan, J.; Zhang, B.; Tao, Z. M.; Fukunaga, C.; Dai, H. J., Ultrafast fluorescence imaging in vivo with conjugated polymer fluorophores in the second near-infrared window. *Nat. Commun.* **2014,** *5*, *4206*.
43. Zade, S. S.; Bendikov, M., Twisting of Conjugated Oligomers and Polymers: Case Study of Oligo- and Polythiophene. *Chem. Eur. J.* **2007,** *13* (13), 3688-3700.
44. Liu, S.; Zhou, X.; Zhang, H.; Ou, H.; Lam, J. W. Y.; Liu, Y.; Shi, L.; Ding, D.; Tang, B. Z., Molecular Motion in Aggregates: Manipulating TICT for Boosting Photothermal Theranostics. *J. Am. Chem. Soc.* **2019,** *141* (13), 5359-5368.
45. Li, Y.; Cai, Z.; Liu, S.; Zhang, H.; Wong, S. T. H.; Lam, J. W. Y.; Kwok, R. T. K.; Qian, J.; Tang, B. Z., Design of AIEgens for near-infrared IIb imaging through structural modulation at molecular and morphological levels. *Nat. Commun.* **2020,** *11* (1), 1255.
46. Liu, S.; Chen, C.; Li, Y.; Zhang, H.; Liu, J.; Wang, R.; Wong, S. T. H.; Lam, J. W. Y.; Ding, D.; Tang, B. Z., Constitutional Isomerization Enables Bright NIR-II AIEgen for Brain-Inflammation Imaging. *Adv. Funct. Mater.* **2020,** *30* (7), 1908125.
47. Pu, K.; Shuhendler, A. J.; Jokerst, J. V.; Mei, J.; Gambhir, S. S.; Bao, Z.; Rao, J., Semiconducting polymer nanoparticles as photoacoustic molecular imaging probes in living mice. *Nat. Nanotechnol.* **2014,** *9* (3), 233.
48. Jiang, Y.; Upputuri, P. K.; Xie, C.; Zeng, Z.; Sharma, A.; Zhen, X.; Li, J.; Huang, J.; Pramanik, M.; Pu, K., Metabolizable semiconducting polymer nanoparticles for second near-infrared photoacoustic imaging. *Adv. Mater.* **2019,** *31* (11), 1808166.
49. Zhang, Z.; Fang, X.; Liu, Z.; Liu, H.; Chen, D.; He, S.; Zheng, J.; Yang, B.; Qin, W.; Zhang, X.; Wu, C., Semiconducting Polymer Dots with Dually Enhanced NIR-IIa Fluorescence for Through-Skull Mouse Brain Imaging. *Angew. Chem. Int. Ed.* **2020,** *59,* 3691.
50. Miao, Y.; Gu, C.; Yu, B.; Zhu, Y.; Zou, W.; Shen, Y.; Cong, H., Conjugated-Polymer-Based Nanoparticles with Efficient NIR-II Fluorescent, Photoacoustic and Photothermal Performance. *ChemBioChem* **2019,** *20* (21), 2793-2799.
51. Hu, R.; Lager, E.; Aguilar-Aguilar, A.; Liu, J.; Lam, J. W. Y.; Sung, H. H. Y.; Williams, I. D.; Zhong, Y.; Wong, K. S.; Peña-Cabrera, E.; Tang, B. Z., Twisted Intramolecular Charge Transfer and Aggregation-Induced Emission of BODIPY Derivatives. *J. Phys. Chem. C* **2009,** *113* (36), 15845-15853.
52. Wan, H.; Yue, J.; Zhu, S.; Uno, T.; Zhang, X.; Yang, Q.; Yu, K.; Hong, G.; Wang, J.; Li, L.; Ma, Z.; Gao, H.; Zhong, Y.; Su, J.; Antaris, A. L.; Xia, Y.; Luo, J.; Liang, Y.; Dai, H., A bright organic NIR-II nanofluorophore for three-dimensional imaging into biological tissues. *Nat. Commun.* **2018,** *9* (1), 1171.

53. Hong, G.; Diao, S.; Chang, J.; Antaris, A. L.; Chen, C.; Zhang, B.; Zhao, S.; Atochin, D. N.; Huang, P. L.; Andreasson, K. I.; Kuo, C. J.; Dai, H., Through-skull fluorescence imaging of the brain in a new near-infrared window. *Nat. Photonics* **2014,** *8* (9), 723-730.
54. Li, Q.; Ding, Q.; Li, Y.; Zeng, X.; Liu, Y.; Lu, S.; Zhou, H.; Wang, X.; Wu, J.; Meng, X.; Deng, Z.; Xiao, Y., Novel small-molecule fluorophores for in vivo NIR-IIa and NIR-IIb imaging. *Chem. Commun.* **2020,** *56* (22), 3289-3292.
55. He, S.; Song, J.; Qu, J.; Cheng, Z., Crucial breakthrough of second near-infrared biological window fluorophores: design and synthesis toward multimodal imaging and theranostics. *Chem. Soc. Rev.* **2018,** *47* (12), 4258-4278.
56. Du, J.; Liu, S.; Zhang, P.; Liu, H.; Li, Y.; He, W.; Li, C.; Chau, J. H. C.; Kwok, R. T. K.; Lam, J. W. Y.; Cai, L.; Huang, Y.; Zhang, W.; Hou, J.; Tang, B. Z., Highly Stable and Bright NIR-II AIE Dots for Intraoperative Identification of Ureter. *ACS Appl. Mater. Interfaces* **2020,** *12* (7), 8040-8049.
57. Shou, K.; Qu, C.; Sun, Y.; Chen, H.; Chen, S.; Zhang, L.; Xu, H.; Hong, X.; Yu, A.; Cheng, Z., Multifunctional biomedical imaging in physiological and pathological conditions using a NIR-II probe. *Adv. Funct. Mater.* **2017,** *27* (23), 1700995.
58. Sun, Y.; Ding, M.; Zeng, X.; Xiao, Y.; Wu, H.; Zhou, H.; Ding, B.; Qu, C.; Hou, W.; Er-Bu, A.; Zhang, Y.; Cheng, Z.; Hong, X., Novel bright-emission small-molecule NIR-II fluorophores for in vivo tumor imaging and image-guided surgery. *Chem. Sci.* **2017,** *8* (5), 3489-3493.
59. Vahrmeijer, A. L.; Hutteman, M.; van der Vorst, J. R.; van de Velde, C. J.; Frangioni, J. V., Image-guided cancer surgery using near-infrared fluorescence. *Nat. Rev. Clin. Oncol.* **2013,** *10* (9), 507-518.
60. Antaris, A. L.; Chen, H.; Cheng, K.; Sun, Y.; Hong, G.; Qu, C.; Diao, S.; Deng, Z.; Hu, X.; Zhang, B.; Zhang, X.; Yaghi, O. K.; Alamparambil, Z. R.; Hong, X.; Cheng, Z.; Dai, H., A small-molecule dye for NIR-II imaging. *Nat. Mater.* **2016,** *15* (2), 235-42.
61. Ou, H.; Cheng, T.; Zhang, Y.; Liu, J.; Ding, Y.; Zhen, J.; Shen, W.; Xu, Y.; Yang, W.; Niu, P., Surface-adaptive zwitterionic nanoparticles for prolonged blood circulation time and enhanced cellular uptake in tumor cells. *Acta Biomater.* **2018,** *65*, 339-348.
62. Gao, H.; Cheng, T.; Liu, J.; Liu, J.; Yang, C.; Chu, L.; Zhang, Y.; Ma, R.; Shi, L., Self-Regulated Multifunctional Collaboration of Targeted Nanocarriers for Enhanced Tumor Therapy. *Biomacromolecules* **2014,** *15* (10), 3634-3642.
63. Jayne, D.; Fook, S.; Loi, C.; Seow-Choen, F., Peritoneal carcinomatosis from colorectal cancer. *Br. J. Surg.* **2002,** *89* (12), 1545-1550.
64. Gu, X.; Zhang, X.; Ma, H.; Jia, S.; Zhang, P.; Zhao, Y.; Liu, Q.; Wang, J.; Zheng, X.; Lam, J. W., Corannulene-incorporated AIE nanodots with highly suppressed nonradiative decay for boosted cancer phototheranostics in vivo. *Adv. Mater.* **2018,** *30* (26), 1801065.
65. Alitalo, A.; Detmar, M., Interaction of tumor cells and lymphatic vessels in cancer progression. *Oncogene* **2012,** *31* (42), 4499-508.
66. Wu, W.; Yang, Y.; Yang, Y.; Yang, Y.; Zhang, K.; Guo, L.; Ge, H.; Chen, X.; Liu, J.; Feng, H., Molecular Engineering of an Organic NIR-II Fluorophore with Aggregation-Induced Emission Characteristics for In Vivo Imaging. *Small* **2019,** *15* (20), 1805549.
67. Li, C.; Zhang, Y.; Wang, M.; Zhang, Y.; Chen, G.; Li, L.; Wu, D.; Wang, Q., In vivo real-time visualization of tissue blood flow and angiogenesis using Ag2S quantum dots in the NIR-II window. *Biomaterials* **2014,** *35* (1), 393-400.
68. Rasmussen, J. C.; Tan, I. C.; Marshall, M. V.; Fife, C. E.; Sevick-Muraca, E. M., Lymphatic imaging in humans with near-infrared fluorescence. *Curr. Opin. Biotechnol.* **2009,** *20* (1), 74-82.
69. Qi, J.; Duan, X.; Liu, W.; Li, Y.; Cai, Y.; Lam, J. W. Y.; Kwok, R. T. K.; Ding, D.; Tang, B. Z., Dragonfly-shaped near-infrared AIEgen with optimal fluorescence brightness for precise image-guided cancer surgery. *Biomaterials* **2020,** *248*, 120036.

TOC

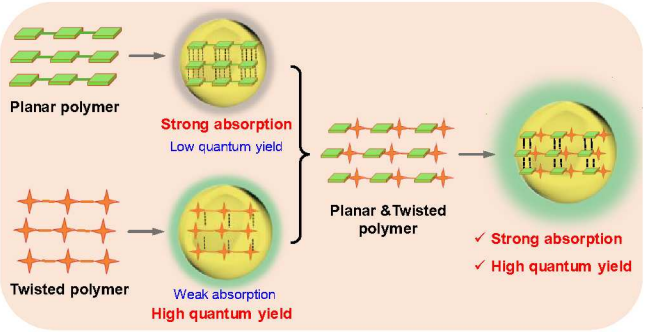
Planar polymer
Strong absorption
Low quantum yield
Twisted polymer
Weak absorption
High quantum yield
Planar &Twisted polymer
✓ Strong absorption
✓ High quantum yield